

Theoretical investigation of halide perovskites for solar cell and optoelectronic applications*

Jingxiu Yang(杨竞秀)^{1,3}, Peng Zhang(张鹏)^{2,3}, Jianping Wang(王建平)³, and Su-Huai Wei(魏苏淮)^{3,†}

¹School of Materials Science and Engineering, Jilin Jianzhu University, Changchun 130118, China

²College of Physics and Optoelectronic Engineering, Shenzhen University, Shenzhen 518060, China

³Beijing Computational Science Research Center, Beijing 100193, China

(Received 17 July 2020; revised manuscript received 21 August 2020; accepted manuscript online 1 September 2020)

The solar cell based on organic-inorganic hybrid halide perovskite is progressing amazingly fast in last decade owing to the robust experimental and theoretical investigations. First-principles calculation is one of the crucial ways to understand the nature of the materials and is practically helpful to the development and application of perovskite solar cells. Here, we briefly review the progress of theoretical studies we made in the last few years on the modification of electronic structures of perovskites by varying the composition, configuration, and structure, and the new understandings into the defect properties of halide perovskites for solar cell and optoelectronic applications. These understandings are foundations and new starting points for future investigations. We hope the experience and inspiration gained from these studies encourage more theoretical explorations for new functional perovskite-based materials.

Keywords: solar cell, optoelectronic properties, defect, halide perovskite

PACS: 84.60.Jt, 71.20.-b, 61.72.J-, 46.25.Cc

DOI: 10.1088/1674-1056/abb3f6

1. Introduction

1.1. Background

Perovskites are a family of materials with the chemical formula ABX_3 , where X is usually chalcogen or halogen. Most of the chalcogenide perovskites, especially oxide perovskites are well-known magnetic, ferroelectric, piezoelectric, and even photocatalytic materials.^[1–4] Recently, halide perovskites have drawn general interest in the field of material science and physics due to the dramatic increase of the power conversion efficiency (PCE) of halide-perovskite-based solar cells from 3.8% to 25.2% during the last decade.^[5–16] In addition to the experimental progress, lots of efforts have been focused on the theoretical study of the perovskite materials for solar cell and optoelectronic applications. In this paper, we will briefly review our theoretical work on the basic electronic structure, property modification, and defects of the perovskite materials.

1.2. Basic properties

The family of halide perovskites contains high-efficient photovoltaic and optoelectronic materials, such as $\text{CH}_3\text{NH}_2\text{PbI}_3$ (MAPbI₃). The excellent performance of the MAPbI₃-based solar cell is mainly due to its exceptional optoelectronic properties: (i) ideal band gap (~ 1.5 eV),^[17] (ii) high light absorbance ($\sim 10^{-5}$ cm⁻¹),^[18] (iii) low exciton binding energy (10–30 meV),^[19] (iv) low and balanced elec-

tron and hole effective masses ($\sim 0.1m_0$),^[20] (v) long-lived charge carrier,^[21,22] and (vi) defect tolerance.^[23,24]

The origin of all the above excellent optoelectronic properties is the special electronic structure of the halide perovskite, such as MAPbI₃, as shown in Fig. 1. The simplest structure of MAPbI₃ is a cubic structure (α phase), where cation Pb^{2+} has six nearest neighbor anions I^- and organic cation MA^+ has twelve nearest neighbor anions I^- . Unlike the 1st and 2nd generation photovoltaic materials (Si or GaAs), the perovskites have an inverted band structure. The valence band maximum (VBM) has anion p , Pb p and s characters; and the conduction band minimum (CBM) has non-bonding Pb p character. The occupied Pb s orbital couples strongly with anion p orbital at R point, leading to direct band gap, low effective mass, and high optical transition matrix elements. Besides, the high degeneracy of the band edge states and s , p wavefunction characters result in high joint density of states (JDOS),^[25] which is responsible for the high absorption coefficient of perovskite compared to GaAs within the visible light range. The strong spin-orbital coupling (SOC) of the heavy atoms Pb and I together with the lack of inversion symmetry results in the Rashba effect, which splits the spin-degenerate bands by shifting their extrema away from the R point. The mismatch of the spin momentum at the splitted VBM and CBM leads to the quasi-direct band structure, which is partly responsible for the low radiative recombination rate in the system.^[21,22]

*Project supported by the National Key Research and Development Program of China (Grant No. 2016YFB0700700), the National Natural Science Foundation of China (Grant Nos. 51672023, 11634003, and U1930402), and the Creative Talents Plan in CPSF, China (Grant No. BX2018033).

†Corresponding author. E-mail: suhuaiwei@csrc.ac.cn

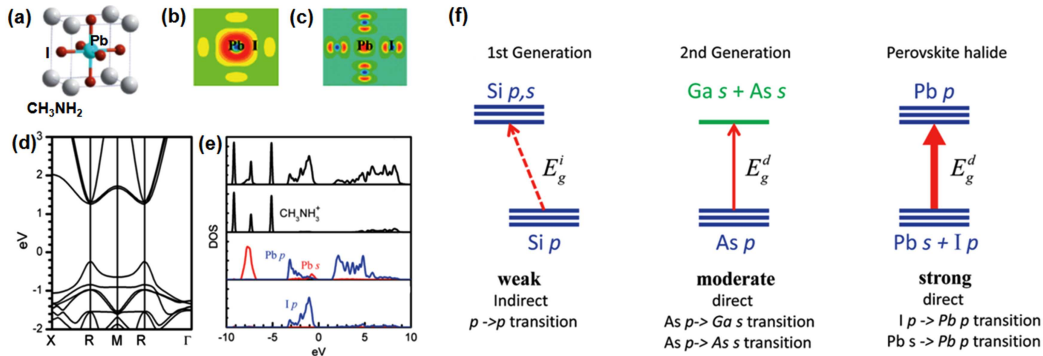


Fig. 1. The crystal structure of (a) α phase MAPbI_3 , (b) partial charge density of the CBM, (c) partial charge density of the VBM, (d) band structure, (e) density of states (DOS) and partial DOS of MAPbI_3 . (f) Schematic optical absorption of Si, GaAs, and halide perovskites. Modified with permission from Ref. [17].

The formation and property of the intrinsic defects in perovskites have also been well studied as shown in Fig. 2. The low energy defects such as V_{MA} , V_{Pb} , MA_{Pb} , MA_{I} , I_i , MA_i have shallow defect levels, whereas the defects with deep defect levels (I_{MA} , I_{Pb} , Pb_{I} , Pb_i , and etc.) all have high formation energy. In other word, most of the formable intrinsic defects are shallow defects. Besides, the halide perovskites could either be p-type or n-type depending on the chemical potential,

which is quite beneficial to the diversity of the growth approaches and solar cell architectures.^[26] This observed “defect tolerance” originates from the large atomic size of the elements and the ionic character of the compounds with ionization state $q = \pm 1$. Recently, some studies have suggested that some charged defects can act as recombination centers in halide perovskites.^[27–29] We will review and discuss this issue in detail in Section 3.

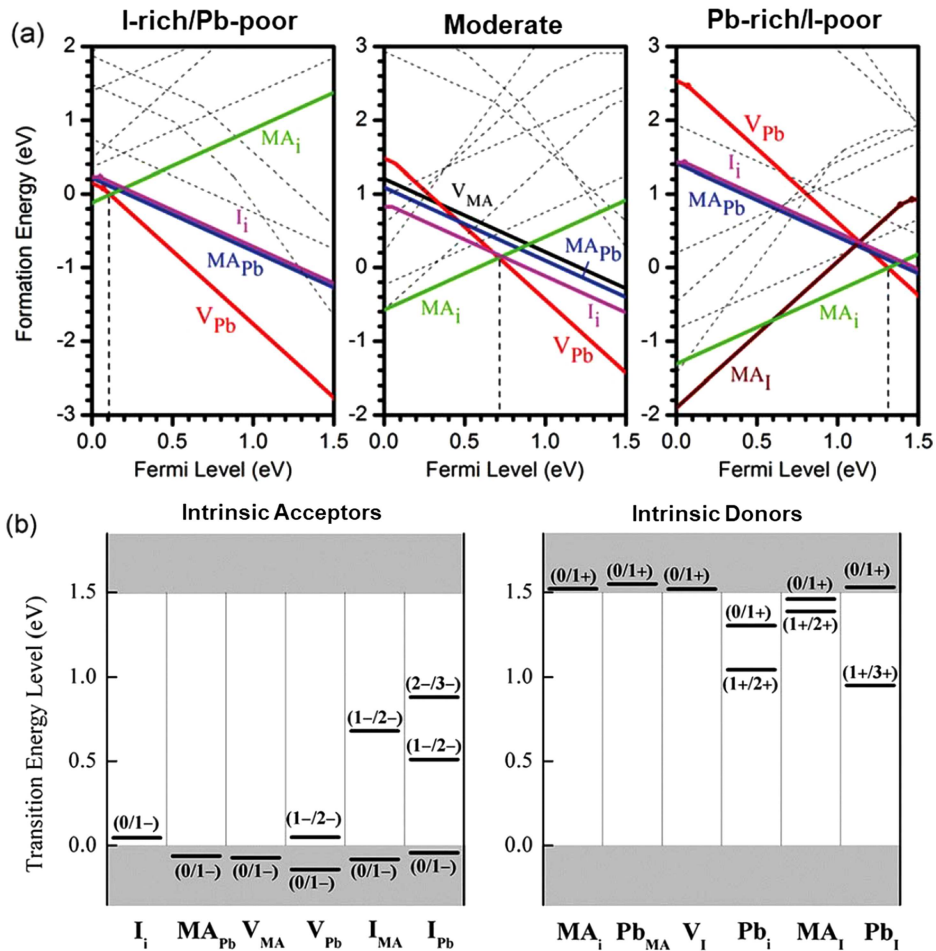


Fig. 2. The formation energies (a) and the transition energy levels (b) of intrinsic point defects in MAPbI_3 under the condition of different chemical potentials. Defects with much higher formation energies are displayed as dashed lines. Zero in energy is referred to the VBM. Modified with permission from Refs. [17,23].

1.3. Disadvantages and solution

Despite the exceptional optoelectronic properties of organic-inorganic hybrid halide perovskites, two serious problems including thermodynamic instability of MAPbI₃ and toxicity of the water soluble Pb²⁺ ions have presented major barriers to their commercial application.^[30,31]

The low stability of MAPbI₃ was once attributed to the moisture, oxygen, UV-radiation, and heat in the environment.^[7,32,33] However, first-principles calculations show that MAPbI₃ in the α (*Pm* $\bar{3}m$), β (*I4/mmc*), and γ (*Pnma*) phase is thermodynamically unstable and will eventually decompose, although it could be synthesized.^[34] The thermodynamic stability is closely related to the geometric tolerance factor t ($t = (R_A + R_X)/\sqrt{2}(R_B + R_X)$), which should be close to 1 in principle. For MAPbI₃ in α phase, $t \geq 0.89$ at finite temperature.^[35] To enhance the stability, t is required to increase towards 1. Given this, altering the effective radius of *A*, *B*, or *X* to adjust the tolerance factor is a possible solution to the issue. Another way to enhance the stability is to convert the crystal structure but retain the excellent electronic structure, which will be discussed in Subsection 2.3.

The other problem relates to the toxicity of lead. To solve the problem of toxicity, the concept of Pb-free perovskite was therefore introduced. A direct way to solve the problem is to replace Pb²⁺ by another cation with similar lone-pair state such as Sn²⁺ or Ge²⁺. Substituting Pb by Sn/Ge is expected to increase the tolerance factor t and improve the thermodynamic stability. Whereas, the stability of Sn²⁺/Ge²⁺ in halide perovskite is a challenge because of the easy oxidization of Sn²⁺/Ge²⁺ into Sn⁴⁺/Ge⁴⁺ (if without protection) in Sn/Ge based halide perovskites.^[36–38] To date, the PCE of the Sn-based halide perovskite solar cell has just achieved 10%.^[39] Instead of entirely substituting Pb by Sn, mixed-(Sn,Pb) perovskite could reduce the amount of used Pb, while tuning the bandgap and retaining the stability.^[38,40,41] Another way to develop Pb-free perovskites is to replace a pair of Pb²⁺ with one B₁⁺ and one B₂³⁺ to form double perovskite.^[42,43] With different combinations of B₁ and B₂, electronic structures and optoelectronic properties are tunable. In addition, altering the configuration with fixed composition and structure could also adjust its properties, which will be discussed in Subsection 2.2.

2. Property modification and control

To overcome the disadvantages of MAPbI₃ and search for the stable Pb-free perovskite materials, property modification and control based on perovskites have been carried out by altering the composition, configuration, and structure. The following works describe several ways to control and adjust the properties and show the great potential and various possibilities of perovskite materials.

2.1. Variation of composition

Altering and adjusting composition is usually an effective way to modify the optoelectronic properties of materials. The easiest way to adjust the composition is to introduce a new element on an ion site. For ABX₃ perovskite, the synthesis and application of mixed-(Sn,Pb) perovskites have already verified the feasibility of the composition mixing on *B*-site. Our studies of ion mixing on the *A*- and the *X*-sites show that the compositional management of ions on *A*- or *X*-site not only modifies the optoelectronic properties but also increases the stability of the halide perovskite.^[44,45] The compositional adjustment is not limited to merely one certain ion-site but can extend to all ion-sites in ABX₃. Here, we take the high-throughput screening of chalcogenide perovskites as an example to show the property modification, especially the stability improvement, by altering the entire composition.^[46]

2.1.1. The *A*-site cation mixing

As mentioned in Subsection 1.3, Goldschmidt tolerance factor t is one of the important empirical indexes for predicting stable crystal structures of perovskite materials. As shown in Fig. 3, a t value between 0.8 and 1.0 is favorable for cubic perovskite structure, and larger (> 1) or smaller (< 0.8) values of tolerance factor usually result in non-perovskite structures. For example, CH(NH₂)₂PbI₃ (FAPbI₃) can exist in the perovskite α -phase (CaTiO₃-type) with good photovoltaic properties. However, it is more stable in the hexagonal phase (CsNiBr₃-type) with $t > 1$.^[47] On the other hand, CsPbI₃ is stabilized to an orthorhombic structure (NH₄CdCl₃-type) with $t < 0.8$.^[48] Combined first-principles calculations and experimental observation show that by alloying FAPbI₃ with CsPbI₃, the effective tolerance factor could be tuned, and the stability of the photoactive α -phase of the mixed solid-state perovskite alloys FA_{1-x}Cs_xPbI₃ is enhanced.^[44]

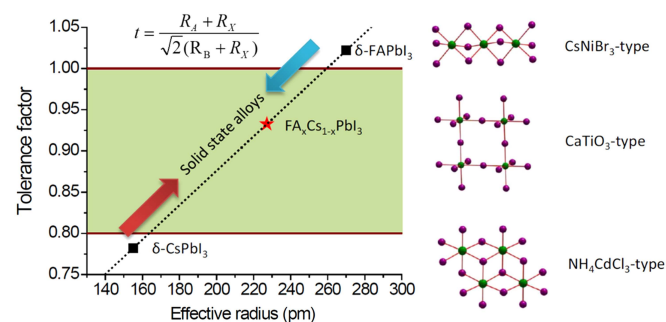


Fig. 3. Correlations between tolerance factor and crystal structure of perovskite materials. Reprinted with permission from Ref. [44].

Recently, people realize that this classic tolerance factor t is often insufficient to predict the stability of perovskites. To enhance the accuracy of this descriptor, amendments have been applied to the classic equations.^[49,50] So far, the tolerance factor t (with or without revision) is closely checked in

studying the thermodynamic stability and the strategy of alloy induced enhancement of stability is commonly adopted for high performance perovskite-based solar cell. [11,51–56]

2.1.2. The X-site anion mixing

Mixing multiple halogen ions is expected to have at least three beneficial effects including enhancing the stability, improving the carrier transport, and the band gap tuning. [6,9,57–63] However, the statistical relationship of basic electronic and structural properties corresponding to the mixing composition was not clear. Therefore, we took $\text{CsPb}(X_{1-x}Y_x)_3$ ($X, Y = \text{I}, \text{Br}, \text{Cl}$) as example to study the alloy properties of mixed halogen anions. As shown in Fig. 4(a), the volume variation is normally linear to the concentration. Whereas, the variations of formation energies and band gaps of the mixed random halide alloys $\text{CsPb}(X_{1-x}Y_x)_3$ show unusual behaviors. The band gap bowing is negligible or even negative (in agreement with experimental results denoted as crosses, pluses, and green stars marks) possibly because the interband coupling cancels the intraband coupling, which is usually observed in conventional

semiconductors. The formation energy is positive for random alloys simulated using the standard quasi-random structure (SQS) approach, but could be very small or even negative for some ordered alloys at some concentrations ($x = 1/3$) as shown in Fig. 4(a) by triangles. The calculated formation energies of the ordered anion alloy $\text{CsPbI}_2\text{Br}_1$, $\text{CsPbI}_2\text{Cl}_1$, and $\text{CsPbBr}_2\text{Cl}_1$ were -5 meV, 4 meV, and -7 meV per formula unit, respectively. Usually, mixing multiple ions will cost energy due to the strain effect. This also explains why formation of mixed-(I, Cl) alloy is difficult but forming mixed-(Br, Cl) and (I, Br) alloys is easier. However, the Coulomb interaction of the isoivalent halogen ions is negative as shown in Fig. 4(b). With combined effects of strain and Coulomb interactions, the very stable ordered structure CsPbX_2Y_1 is therefore expected to form as shown in Fig. 4(c). To date, the anion alloyed halide perovskites are commonly used to enhance the stability and the efficiency for single and tandem perovskite solar cells. [64–69] Particularly, the proposed ordered CsPbI_2Br perovskite solar cell achieves an efficiency of 16.79% with high air stability in this year. [70]

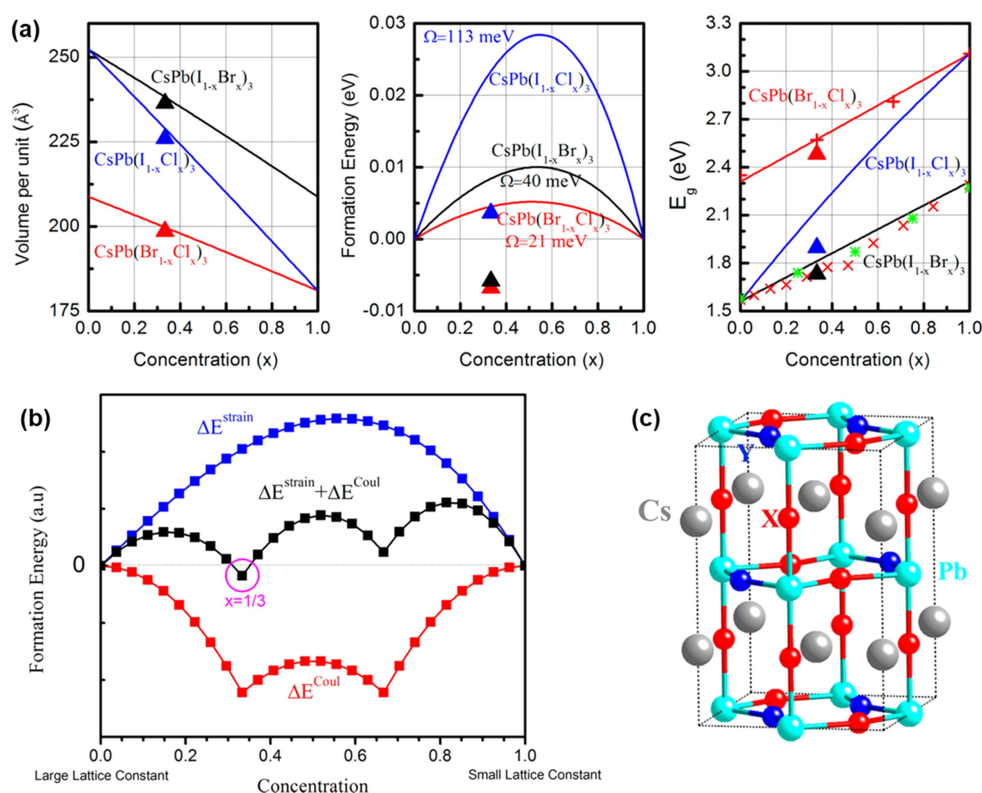


Fig. 4. (a) Variations of volumes, formation energies (per halogen atom), and band gaps of the mixed halide alloys $\text{CsPb}(X_{1-x}Y_x)_3$ ($X, Y = \text{I}, \text{Br}, \text{Cl}$) by SQS calculation. The solid lines are fitted by calculated results of SQS at nine different concentrations (fitted points are not shown for clarity). The triangles represent the stable ordered structures at $x = 1/3$. For band gaps, the available experimental data are given (red cross marks are data from Ref. [71], the red plus marks are data from Ref. [58], and the green star marks are data from Ref. [63]). (b) The contributions of strain energy and Coulomb energy in the alloy. (c) Particularly stable mixed-halide structures for CsPbX_2Y_1 ($X, Y = \text{I}, \text{Br}, \text{Cl}$; the atomic size of X is larger than Y). Reprinted with permission from Ref. [45].

2.1.3. The thorough composition management for ABX_3

Motivated by the common sense that chalcogenides are more stable than halides because of their higher Coulomb in-

teraction energy, it is worthy to investigate whether there are applicable chalcogenide perovskites for solar cells. The previous reported works proposed the possibility of chalcogenide perovskites such as BaZrS_3 , CaTiS_3 , CaZrSe_3 , CaHfSe_3 ,

SrSnS₃, and SrSnSe₃ as solar cell absorbers based on theoretical investigation of very limited number of ABX_3 compounds.^[72–74] To systematically screen all the possible compositions of ABX_3 for solar cell absorber, high-throughput first-principles calculations were performed to extensively investigate 168 ABX_3 chalcogenide compounds ($A = \text{Mg, Ca, Sr, Ba, Zn, Cd, Sn, Pb}$; $B = \text{Ti, Zr, Hf, Si, Ge, Sn, Pb}$; $X = \text{O, S, Se}$) in fixed four different crystal structures (as shown in Fig. 5(a)), with a total of 672 systems, for potential applications as solar cell absorbers. Based on screening criteria such as phase stability (thermodynamic and dynamic), band gap, carrier effective mass, and optical absorption, five possible candidates BaZrS₃, BaZrSe₃, SrZrSe₃, BaHfSe₃, and SrHfSe₃ were identified for potential solar cell applications,

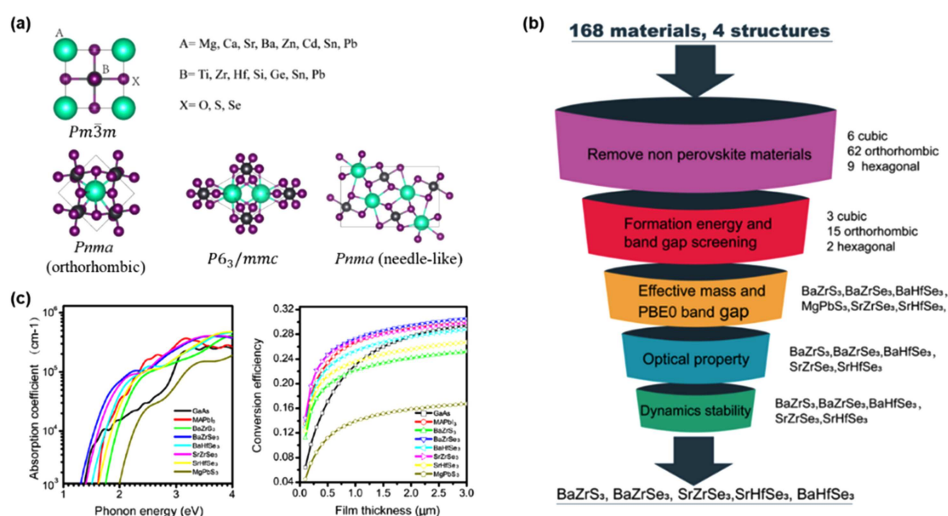


Fig. 5. (a) Four common structures for ABX_3 compounds as denoted. (b) Screening progress. (c) Calculated optical absorption coefficients and conversion efficiencies of six types of perovskites, MAPbI₃, and GaAs. Reprinted with permission from Ref. [46].

2.2. Variation of configuration

Altering and adjusting the atomic configuration with fixed crystal lattice and chemical formula could also lead to the variation of the electronic band structure, the thermodynamic and optoelectronic properties. Given this general recognition, efforts have been made to refine the aimed property by changing the ordering of atomic configurations. However, the variation from ordered structure to disordered structure usually costs energy. If the ground state is not stable, it is meaningless to discuss varying the configuration. For ABX_3 perovskites, even regardless the problem of the intrinsic instability, the variation of the configuration of the A and B cations is quite limited because the symmetry and the coordination of A and B are entirely different in the compound.

Cation-transmutation is an effective method to enlarge the selectivity and diversity of materials. Cation-transmutation is a sequential process involving a series of cation mutations to keep the overall number of valence electrons maintained and the compound remains charge neutral. The transmutations of the class of I–III–VI₂ and I₂–II–IV–VI₄ photo-

voltaic materials from II–VI semiconductors are successful examples.^[79–81] When the number of cations increases in the compound, more different ordered or disordered cation atomic configurations are possible in the sample. Also, the electronic structures can depend sensitively on the atomic configuration. In this section, we will introduce the design of the electronic band structure of inorganic double perovskite by cation transmutation.^[42,82] and the effect of configuration variation on the material properties.^[83]

as shown in Fig. 5(b). The identified compounds are dynamically stable at 300 K, their band gaps and carrier effective masses are appropriate, and they can achieve comparable or even higher efficiency than MAPbI₃ due to the strong p–d transition (Fig. 5(c)). Later, BaZrS₃ has been synthesized in experiment and further studied. The synthetic powder of BaZrS₃ possesses the $Pnma$ space group with a direct band gap of 1.73–1.85 eV,^[75–77] which is obviously wider than the optimal band gap for PVs. To reduce the band gap, two strategies including alloying Ti at the Zr site and mixing Se to the S site were proposed.^[75] It is finally found that the former strategy is more effective for band gap reduction, only a 4 at.% alloying decreases the band gap from 1.78 eV to 1.51 eV.^[78] However, higher Ti-alloying concentration leads to destabilization.^[76,78]

voltaic materials from II–VI semiconductors are successful examples.^[79–81] When the number of cations increases in the compound, more different ordered or disordered cation atomic configurations are possible in the sample. Also, the electronic structures can depend sensitively on the atomic configuration. In this section, we will introduce the design of the electronic band structure of inorganic double perovskite by cation transmutation.^[42,82] and the effect of configuration variation on the material properties.^[83]

2.2.1. Cation transmutation

To counteract the mentioned two key issues of hybrid organic–inorganic halide perovskites, people have searched alternative high-performance stable Pb-free photovoltaic materials. One of the strategies is using cation-transmutation to design stable inorganic Pb-free halide perovskites for solar cells. The idea is to convert two divalent Pb²⁺ ions into one monovalent B₁⁺ and one trivalent B₂³⁺ ions, forming a rich class of quaternary halides in double-perovskite structure, as shown in Fig. 6(a). The B₁⁺ and B₂³⁺ share the equivalent symmetry

and coordination environment, and therefore the atomic configurations of the two cations directly influence the energy of the material. After checking the energies for all the possible first-neighbored arrangements of B_1X_6 and B_2X_6 octahedra, the ground state structure denoted F was finally obtained as shown in Fig. 6(b). With photovoltaic-functionality-directed materials screening in Fig. 6(c), 11 optimal materials with intrinsic thermodynamic stability, suitable band gaps, small carrier effective masses, and low excitons binding energies were preliminarily identified as promising candidates to replace Pb-

based photovoltaic absorbers in perovskite solar cells. As shown in Fig. 6(d), many compounds in double perovskites have good phase stability against decomposition into binary and ternary compounds. It was proposed that $Cs_2InSbCl_6$ and $Cs_2InBiCl_6$ could be representative double perovskites for solar cell applications based on the strict criteria and assumption that In^+ can be stable. However, it was pointed out that the easy oxidation of In^+ to In^{3+} can lead these proposed double perovskites unstable.^[84]

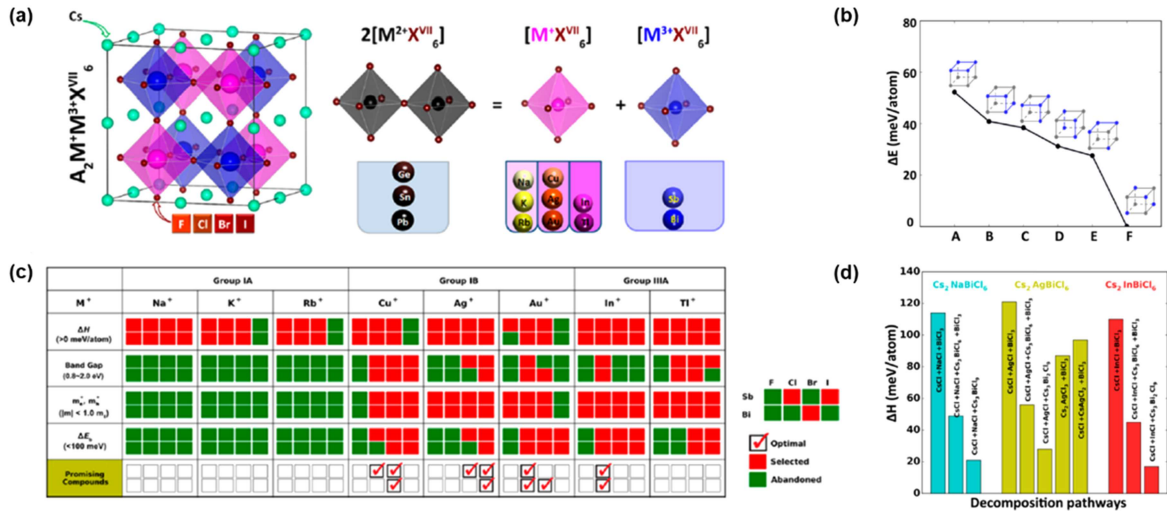


Fig. 6. (a) Schematic idea of atomic transmutation and candidate $A_2B_1^+B_2^{3+}X_6^{VII}$ perovskites for materials screening. (b) Energies of $Cs_2AgBiCl_6$ with different arrangements of $AgCl_6$ (in gray) + $BiCl_6$ (in blue). The energy of the lowest configuration F is set to zero. (c) Materials screening process by considering the properties relevant to photovoltaic performance, such as decomposition enthalpy (ΔH), band gap, effective masses (m_e^* , m_h^*), and exciton binding energy (ΔE_b). The red squares mean the materials passing the screening (selected) and the green ones mean not passing (abandoned). The optimal nontoxic $A_2B_1^+B_2^+X_6$ perovskites satisfying all the criterions are marked with red checks. (d) The ΔH corresponding to different decomposition pathways for selected $A_2B_1^+B_2^{3+}X_6$. Reprinted with permission from Ref. [42].

Later, several other candidates have been proposed, both experimentally and theoretically, which include various combinations of $A_2B_1^+B_2^{3+}X_6$ such as Cs_2SnI_6 ,^[85–88] Cs_2AgBiX_6 ($X = Br, Cl$),^[89–92] $Cs_2InAgCl_6$,^[93] $Rb_2CuInCl_6$ ($Rb_2AgInBr_6$),^[94] etc. Guidelines were urgently required for the rational development of stable Pb-free double perovskites. To fill in the gap, a systematic study on the relationship between B_1^+/B_2^{3+} combination and its electronic structures was carried out by the authors.^[82] The possible candidates of B_1^+/B_2^{3+} cations can be classified into three classes by their valence atomic components: those with the d states, those with lone pair s state, and those without the d or s states. Considering the possible combinations of the three classes of the B_1^+/B_2^{3+} cations, six distinct families of halide double perovskites were found, as shown in Fig. 7. Based on the symmetry analysis of the band structure, we found that both the B_1^+/B_2^{3+} cations in $A_2B_1^+B_2^{3+}X_6$ must possess the lone-pair s states (Fig. 7(h)). Thus, there is strong s-p coupling between the lone-pair s and X p orbitals in the valence band and there is no strong s-p coupling in the conduction band. To satisfy this criterion, the class of $A_2B_1^{IIIA}B_2^{VA}X_6$ compounds suffered from the instability issue was the only possible candidates based on

the band structure analysis. This put the idea of Pb-free double perovskite for solar cell into a dilemma. Despite this, halide double perovskites have good material properties that go beyond solar cells. Indeed, they have been recently employed for other optoelectronic applications such as x-ray imaging,^[95] UV detectors,^[96] laser material,^[97,98] photocatalysts,^[99] and LEDs.^[100–103]

2.2.2. The ordering effect

Instead of trying to improve the stability of $A_2B_1^{IIIA}B_2^{VA}X_6$ compounds, another way to design Pb free halide perovskites for photovoltaic applications is to modify the optoelectronic properties of halide double perovskites that are intrinsically stable. One typical example is $Cs_2AgBiBr_6$, which is synthesized stable in cubic double perovskite structure, and reported to have an indirect band gap of 1.95 eV or 2.19 eV, respectively.^[104,105] Both the indirect band gap and the corresponding little visible-light harvest suggest its limited application in solar energy conversion. However, introducing cation disorder and manipulating ordering can adjust the electronic structure and the light absorption of $Cs_2AgBiBr_6$.^[83]

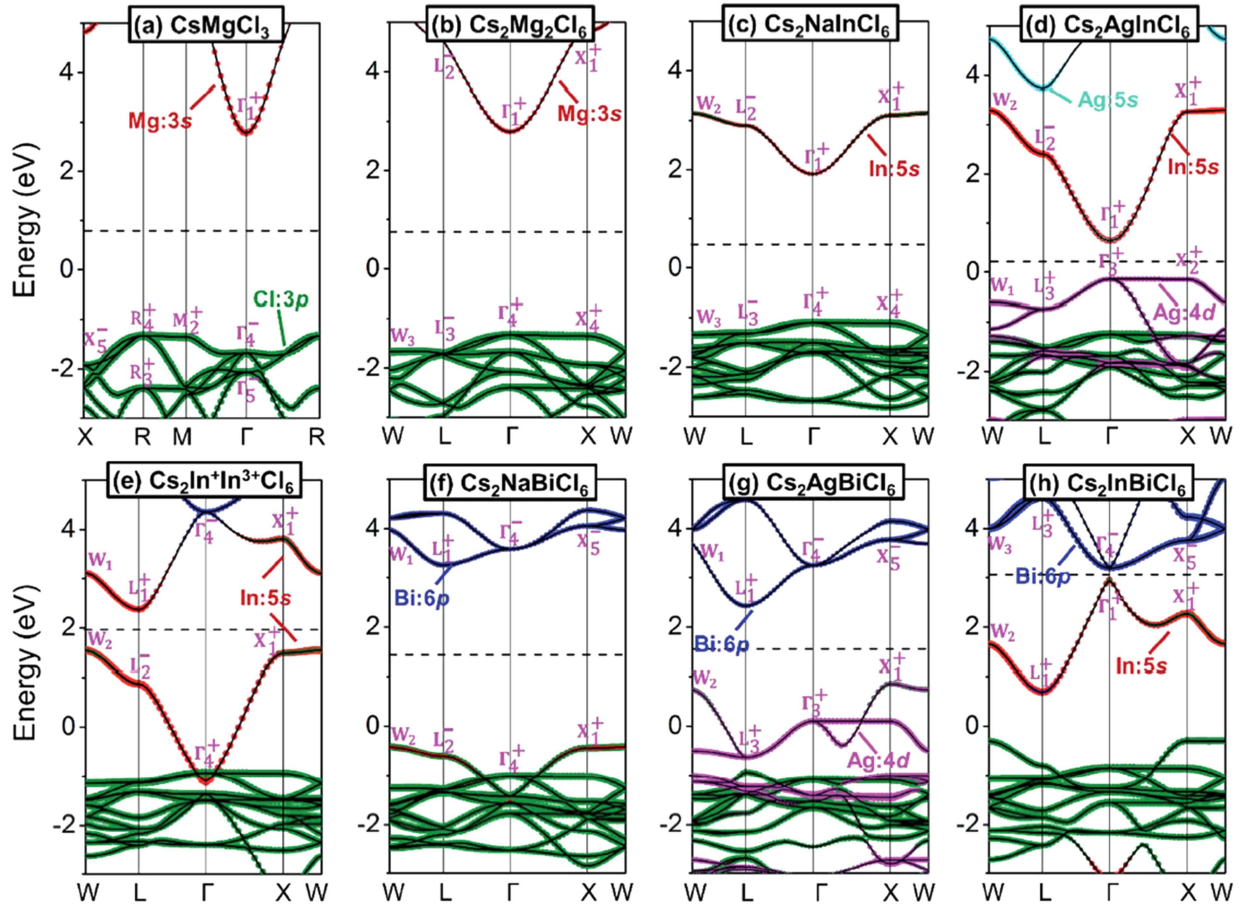


Fig. 7. Calculated band structures for (a) CsMgCl_3 , (b) $\text{Cs}_2\text{Mg}_2\text{Cl}_6$, (c) $\text{Cs}_2\text{NaInCl}_6$, (d) $\text{Cs}_2\text{AgInCl}_6$, (e) $\text{Cs}_2\text{In}^+\text{In}^{3+}\text{Cl}_6$, (f) $\text{Cs}_2\text{NaBiCl}_6$, (g) $\text{Cs}_2\text{AgBiCl}_6$, and (h) $\text{Cs}_2\text{InBiCl}_6$. The s , p , and d orbital components of the bands are represented as red/light blue, green/dark blue, and pink spheres, respectively. All the bands are aligned with respect to the Cs 1s core level. The dashed lines are at the middle of the band gaps. Reprinted with permission from Ref. [82].

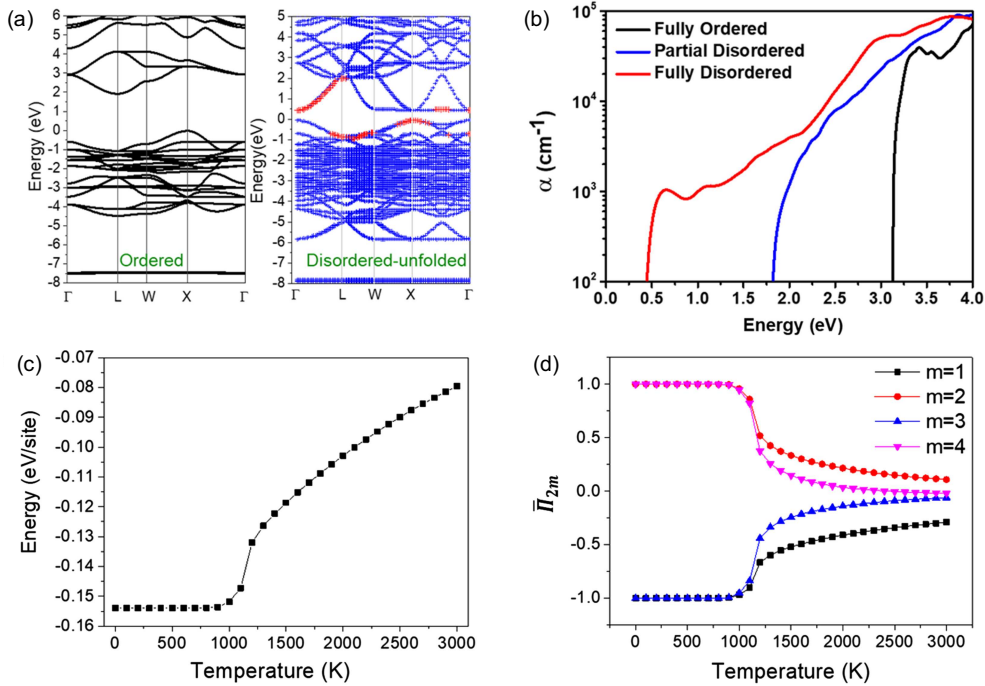


Fig. 8. (a) The band structures of the ordered and fully disordered $\text{Cs}_2\text{AgBiBr}_6$. The red dots represent the band edge states with the spectral weight over 50%. (b) The calculated optical absorption coefficients α (cm^{-1}) of the fully ordered (black), partial disordered (blue), and fully disordered (red) $\text{Cs}_2\text{AgBiBr}_6$. (c) The Monte–Carlo simulation of the excess energy and (d) the corresponding averaged atomic correlation functions of pairs up to the m th neighbor (I_{2m}) as a function of temperature. Modification with permission from Ref. [83].

Comparing the band structures of the ordered and disordered structures, the reduced symmetry in the disordered structure can significantly lower the band gap from 1.93 eV to 0.44 eV and convert the indirect semiconductor to a pseudo-direct one, as shown in Fig. 8(a). The calculated light absorbance in Fig. 8(b) also shows the dramatic red shift of the threshold from 3.13 eV (ordered) to 0.44 eV (fully disordered). The order–disorder transition temperature is estimated to be 1200 K at which sharp changes of the energy and correlation function are observed in Figs. 8(c) and 8(d). The band structure of the partial disordered phase at 1200 K is indirect with a band gap of 1.46 eV and the light absorption threshold is at 1.82 eV in Fig. 8(b). Given the tendency in Figs. 8(c) and 8(d), quenching from appropriate temperature beyond 1200 K, one may synthesize a series of the disordered $\text{Cs}_2\text{AgBiBr}_6$ with the band structures varying from indirect band gap of 1.46 eV to pseudo-direct band gap of 0.44 eV. Varying the ordering configuration not only modifies the size of the band gap but also changes the indirect band gap character to more direct character. Controlling the extent of disorder, the light absorption is considerably enhanced and red-shifted to the visible and the near infrared region for the disordered $\text{Cs}_2\text{AgBiBr}_6$ alloys. The property modification and control of the compound offer an alternative way to develop the stable double perovskites. Indeed, experimentally, partial disordered $\text{Cs}_2\text{AgBiBr}_6$ with the decreased band gap of 1.72 eV was obtained by controlling the temperature and speed of the solution-based crystal growth,^[106] which further confirms the effect of ordering on the band gap.

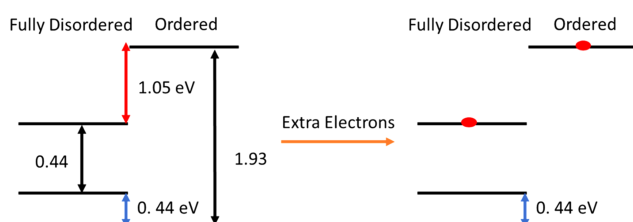


Fig. 9. The schematic idea to stabilize the disordered phase by introducing extra electrons. Modification with permission from Ref. [83].

The order–disorder transition temperature (T_c) is as high as 1200 K due to the large energy difference between the ordered and disordered phases. If the energy difference can be reduced, the synthetic temperature will consequently decrease. As shown schematically in Fig. 9, the CBM of the fully ordered phase is about 1.05 eV higher than that of the fully disordered phase. Introducing extra electrons to the CBM states of the two phases, the disordered phase with the much lower CBM will gain more energy than the ordered phase. In this way, the energy difference between the two phases could be reduced by introducing electrons to the system. To check the proposal, we found that the disordered phase is calculated to be as stable as the ordered phase by substituting 1/8 of Cs with

Ba. If the doping concentration is below 1/8, the energy difference and transition temperature are expected to be decreased.

2.3. Variation of structure

Structural variation is usually expected to cause the interlocked change of the thermodynamic, electronic, and optical properties. For ABX_3 perovskites, we would like to improve the stability and decrease the toxicity without compromising the exceptional optoelectronic properties which are originated from the inverted band structure of the BX_6 octahedron. Therefore, the key issue to modify the target properties is retaining the BX_6 octahedron and including new structural variables. In this section, two schemes including 3D–2D structural conversion^[107] and perovskite–spinel structural conversion^[108] are introduced.

2.3.1. 3D vs. 2D

Creating a surface of a bulk usually costs energy. Therefore, the 3D bulk is often more stable than the corresponding 2D material. To the opposite, reducing the dimension

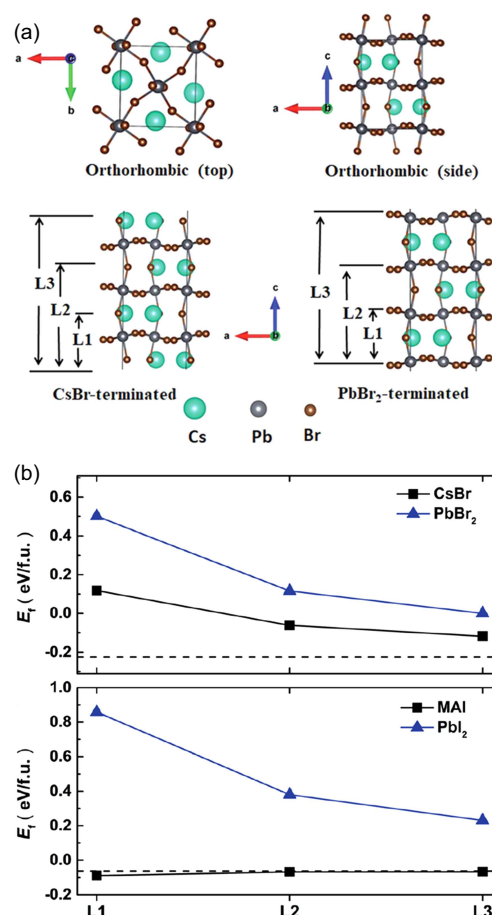


Fig. 10. (a) Top and side views of bulk orthorhombic CsPbBr_3 , CsBr -terminated and PbBr_2 -terminated triple-layer (L3) 2D orthorhombic CsPbBr_3 , respectively. The structures of the monolayer (L1) and double-layers (L2) are indicated. (b) Formation energies (eV/f.u.) of 2D orthorhombic CsPbBr_3 (top) and orthorhombic MAPbI_3 (bottom). Relaxed AX-terminated slabs (squares) and PbX_2 -terminated slabs (triangles) are presented for three different thicknesses, i.e., L1, L2, and L3. The symbols are connected by lines for a better view. The formation energy of bulk APbX_3 is indicated by a horizontal dashed line. Reprinted with permission from Ref. [107].

of the lead halide perovskites from 3D bulk to 2D slabs has been found to improve the stability of the perovskites.^[109–114] This unusual phenomenon that a 2D slab cut out of the 3D bulk could be more stable requires to be understood. Taking MAPbI₃ and CsPbBr₃ as examples (Fig. 10), the PbX₂-terminated 2D APbX₃ are calculated to be less stable than the AX-terminated counterparts because there are more dangling bonds on the PbX₂-terminated surface. For CsPbBr₃, the 3D bulk is more stable than the 2D slab. But the 3D MAPbI₃ bulk is less stable than its MAI-terminated 2D counterpart as shown in Fig. 10(b) due to the structural relaxation of the hydrogen bonds on the surface. Therefore, the enhanced stability of the 2D perovskite is found to originate from the asymmetric surface properties. Our finding provides new insights into the dimension-induced variation of thermodynamic stability.

2.3.2. Perovskite vs. spinel

Tetrahedral coordination semiconductors including crystalline Si, GaAs, CdTe, and octahedral coordination semiconductors, especially perovskites, are two typical classes

of successful semiconductors for solar cell absorbers, as shown in Fig. 11(a).^[115] According to the previous studies, the two classes of semiconductors show complementary properties, which originate from their respective coordination, in terms of bond, stability, light absorption, and defect tolerance.^[23,24,116–118] To combine the advantages of both the tetrahedral and octahedral coordinated semiconductors, a spinel structure is thus proposed as an alternative potential photovoltaic absorber. A publication which studies a class of 315 possible AB₂X₄ systems in three different phases identifies five promising spinel compounds CdIn₂Se₄, HgAl₂Se₄, HgIn₂S₄, HgY₂S₄, and HgSc₂S₄ for solar cells (Fig. 11(b)). Among the five proposed semiconductors, HgAl₂Se₄ with the quasi-direct band structure and a band gap of 1.36 eV (GW0) has a small electron effective mass (0.08m₀), high optical absorption (*p* to *s-p* states), high dynamic stability, and thus is recommended for solar cell application. This work opens a new route and proposes a new class of semiconductors with mixed tetrahedral and octahedral coordinations for emerging solar cell absorbers.

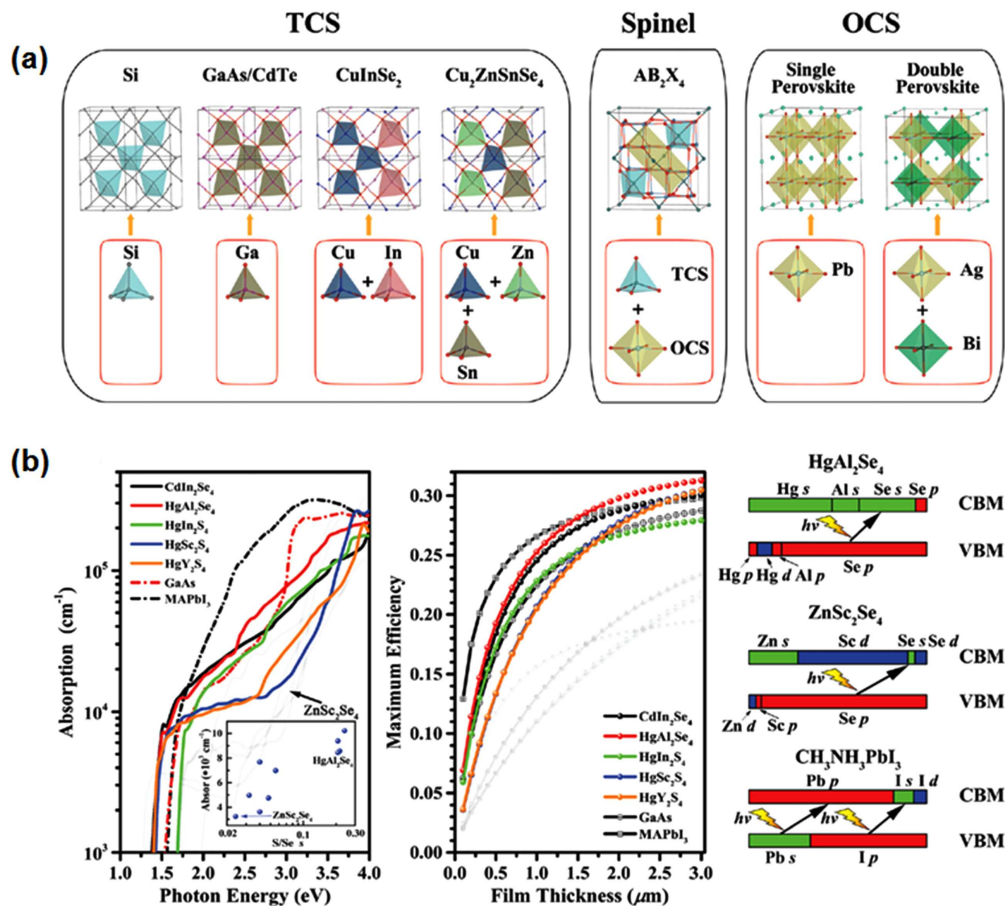


Fig. 11. (a) Representative examples of two classes of structural families for solar cell absorbers of tetrahedral coordination structure and octahedral coordination structure. Spinel structure can be considered as the mixing of tetrahedral and octahedral building blocks but keep high crystal symmetry. (b) The calculated optical absorption spectrum and the spectroscopic limited maximum efficiency (SLME) for 10 spinel compounds MgIn₂Se₄, ZnSc₂Se₄, ZnY₂Se₄, CdSc₂Se₄, CdY₂Se₄, HgAl₂Se₄, HgIn₂S₄, CdIn₂Se₄, HgSc₂S₄, and HgY₂S₄, in comparison to typical solar cell absorbers GaAs and CH₃NH₂PbI₃. Five compounds with inferior performance (MgIn₂Se₄, ZnSc₂Se₄, ZnY₂Se₄, CdSc₂Se₄, and CdY₂Se₄) have been shaded. The orbital character of VBM and CBM for three selected compounds, HgAl₂Se₄, ZnSc₂Se₄, and CH₃NH₂PbI₃. The dipole-allowed intra-atomic transitions are indicated. Reprinted with permission from Ref. [108].

3. Defect and dopants

Defect and dopant directly decide the carrier density and the recombination rate, therefore, are crucial to the efficiency of an optoelectronic device. As we have already stated in Subsection 1.2, the common formable intrinsic defects in the prototype perovskite MAPbI₃ are bipolar and shallow.^[23–25] However, there are also some special cases and different opinions.^[27,28,119] Agiorgousis *et al.* reported the possibility of forming covalency-induced Pb dimers or I trimers with deep transition levels. The Pb dimers and I trimers are only stabilized in a particular charge state with significantly lowered energy, which leads to deep charge-state transition levels within the band gap.^[27] Du used hybrid functional with SOC calculation and found that only the iodine interstitial and its complexes (I_{MA}) could induce deep electron and hole trapping levels inside the band gap acting as nonradiative recombination centers.^[119] Meggiolaro *et al.* also used HSE06 with SOC to recalculate the intrinsic defects in MAPbI₃ and identified I_i⁻ as the deep hole trap state. They proposed that interstitial I_i⁻ can oxidized into I_i⁺ (I trimer) which behaves as a kinetically inactive electron trap state by the chemical post treatment.^[28] The defect properties are quite complicated and more thorough investigations and new understandings are still in progress. Here, we describe some of our new findings regarding the n-

type and the p-type doping in halide perovskite.^[29,120,121]

3.1. Killer defects for n-type doping in perovskites: The DY centers

Substituting Pb with Bi (Bi_{Pb}) is expected to act as a shallow donor to enhance the electron conductivity for optoelectronic materials such as MAPbI₃ and MAPbBr₃ in experiments, because Bi is at the right hand side of Pb in the periodic table.^[122,123] However, suppressed photoluminescence (PL), short photocarrier lifetime, and negative photoconductivity (NPC) were reported for Bi-doped MAPbBr₃ by three different experimental groups.^[120,124,125] The unusual experiment observations of Bi_{Pb} should be correlated to deep defects, which is contrary to empirical expectation. In particular, the NPC is quite rare and might be related to a special case of defect complex. Learning from the donor-derived complex center (DX center) in tetragonal semiconductors, which is a deep negatively charged defect complex converted from a nominally shallow donor defect,^[126–130] the Bi_{Pb} defect in MAPbBr₃ might be a DX-like center, which we denoted it as a DY center (in octahedral semiconductors) in our publication. To figure out whether the unusual defect is DY center, we have systematically investigated the Bi_{Pb} defect in MAPbBr₃ and MAPbI₃, respectively.

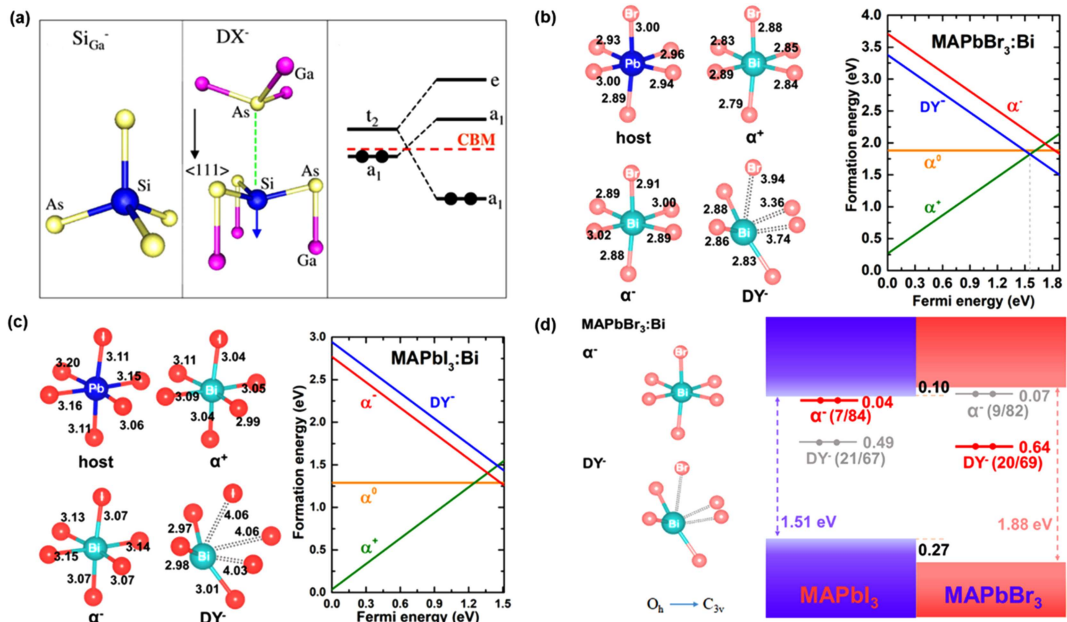


Fig. 12. (a) The schematic illustration of DX center in tetragonal semiconductor. The local structures of the host and α^+ , α^- , and DY^- defect states and the calculated defect formation energy of Bi_{Pb} in (b) Bi-doped MAPbBr₃ and (c) Bi-doped MAPbI₃ as a function of Fermi energy E_F under the anion-rich/Pb-poor condition. The numbers indicate the obtained bond lengths for the full lines or distances for the dotted lines of the broken bonds. (d) The alignment of the band edges of MAPbI₃ and MAPbBr₃ and the relative single electron energy levels of α^- and DY^- states. The red lines represent the stable states, while the grey lines represent the metastable states. The numbers in brackets represent the projected p orbital percentage of (anion/cation). Modification with permission from Refs. [29,130].

As shown in Fig. 12(b), Bi_{Pb} shows the negative- U behavior and might induce DY center in MAPbBr₃. When the Fermi energy E_F is below the crossing point (1.55 eV), the positive α^+ is thermodynamically favorable. When the E_F exceeds

1.55 eV, the localized DY^- state which is highly distorted by breaking three coordination bonds is dominant. To the contrary, Bi_{Pb} shows the positive- U behavior and DY center is not favorable to form in MAPbI₃ (Fig. 12(c)). The α^+ and

α^0 states are stable unless the E_F reaches 1.48 eV. Even forming the negative charged defect, the DY^- state is not stable with respect to α^- in $MAPbI_3$. The origin of the formation of DY center in $MAPbI_3$ and $MAPbBr_3$ is further revealed. As shown in Fig. 12(d), converting from the α^- state to the deep DY^- state, it gains electronic energy by moving the two occupied electrons from the α^- state to the deep DY^- state, and costs strain energy for the structural displacement from the O_h to C_{3v} symmetry. The higher CBM of $MAPbBr_3$ leads to higher electronic energy gain in $MAPbBr_3$, which explains why DY^- state is stable in $MAPbBr_3$ instead of $MAPbI_3$, and why the DY center prefers to form when the CBM of the host is high. The thorough discussion of the DY center thus supplies valuable insights for the defect studies in perovskites and other octahedral semiconductors.^[131,132]

The observed suppressed PL and short lifetime of the electron can be easily understood. Electron trapping or non-radiative recombination are expected to occur once the DY center forms, because the DY^- states are deep enough to act as the trapping center. The mechanism of the NPC in $MAPbBr_3$

can also be explained as seen in Fig. 13. In dark state, Bi_{Pb} is dominantly in α^+ state and shows the character of shallow donor (Fig. 13(a)). Upon light illumination, electrons are excited from the VBM to the CBM, which results in the increase of the photocurrent from A to B in Fig. 13(c). Once the density of electrons is high enough, the quasi-electron Fermi energy (ϵ_{fn}) would shift beyond the crossing point of α^+ state and DY^- state as shown in Fig. 13(d), therefore, the α^+ state starts to convert into the DY^- state (C in Fig. 13(b)) by conquering the energy barrier of 0.17 eV (Fig. 13(f)). After the transition, the trapped electrons in the DY^- states are deep enough to recombine with the holes from the VBM by non-radiative recombination, which thus leads to the fast decay of the photocurrent from C to D in Fig. 13(c). When the light is off, the photocurrent is consequently decreased (E in Fig. 13(c)) as well as the Fermi energy level. The already formed DY center requires layback time to convert back to the α^- or α^+ state conquering the barrier of 0.45 eV, which gives rise to the increase of the current from E to F in Fig. 13(c).

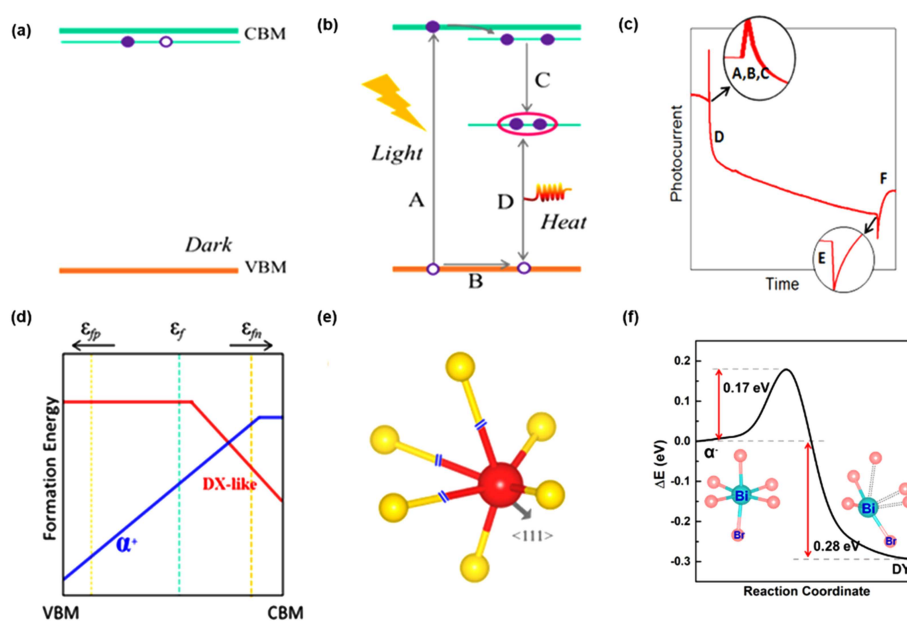


Fig. 13. (a) Schematic diagram of energy levels of the Bi-doped $MAPbBr_3$ crystal in dark. (b) Schematic representation of the emergence of DX-like (DY) defect levels under light illumination. Also shown are the dynamic photocarrier generation and recombination processes that lead to the negative photoconductivity. (c) Negative photoconductivity curve corresponding to the transitions taking place relevant to DY center under light. (d) Schematic plot of formation energies of a shallow donor Bi_{Pb} (α^+) and DY center in $MAPbBr_3$ as functions of the Fermi level (ϵ_f). (e) Atomic configuration of the DY center in Bi-doped $MAPbBr_3$. (f) The transition of Bi-doped $MAPbBr_3$ from the metastable α^- state to the stable DY^- state. Modification with permission from Refs. [29,120].

3.2. P-type doping in perovskite: Transparent conducting materials

Transparent conductors (TCs) have a wide range of applications in optoelectronic devices, such as flat-panel displays, solar cells, transparent thin-film transistors, light-emitting diodes, and touch-screen sensors.^[133–139] However, in these days, the commercially used TCs are mostly based on n-type oxides (TCOs), such as Sn doped In_2O_3 and Al doped ZnO , while the fabrication of their p-type counterparts remains a big challenge. In a recent work, we have proposed a series of

inorganic metal halide perovskites (IMHPs) as potential candidates as p-type TCs, which possess an “inverted band structure (IBS)” compared to conventional n-type TCOs, i.e., having s -like valence band maximum (VBM) and p -like conduction band minimum (CBM) (see Fig. 14(a)). Benefit from this characteristic IBS, these IMHPs can satisfy most criteria of p-type TCs, such as good transparency, high conductivity, good dupability, and high thermodynamic stability.

Taking $CsPbCl_3$ as an example, the calculated band gap is 2.83 eV by HSE06 and GW+SOC methods, which can pro-

hibit the interband absorptions of most visible light in this material (T1 in Fig. 14(b)). Moreover, the VB states at the high-symmetry R -point were found to have the same parity (Fig. 14(c)), which implies that the dipole transitions between these VB states should be forbidden. Consequently, it can be expected that the intraband optical absorptions would also be weak as the material is heavily doped with holes (T2 in Fig. 14(b)). On the other hand, due to the IBS with s -like VBM, CsPbCl₃ has a relatively small m_h^* ($\sim 0.21m_0$), which is comparable to the electron effective masses in conventional n-type TCOs (typically 0.20–0.35 m_0).^[139] This small m_h^* would

guarantee good conductivity in p-type doped CsPbCl₃. As one important feature of TCOs, the p-type dopability of CsPbCl₃ should be high. As shown in Fig. 14(d), the theoretical calculations indicate that it is quite easy to dope CsPbCl₃ p-type by carefully selecting proper dopants, such as Na and K. These extrinsic dopants prefer to substitute Pb in CsPbCl₃ with low formation energies and both yield shallow acceptor levels. Besides CsPbCl₃, other 27 candidates in this IMHPs family were also considered. Among them, RbPbCl₃ and CsPbBr₃ were predicted to be potential candidates as high-performance p-type TCOs, due to their similar properties to CsPbCl₃.

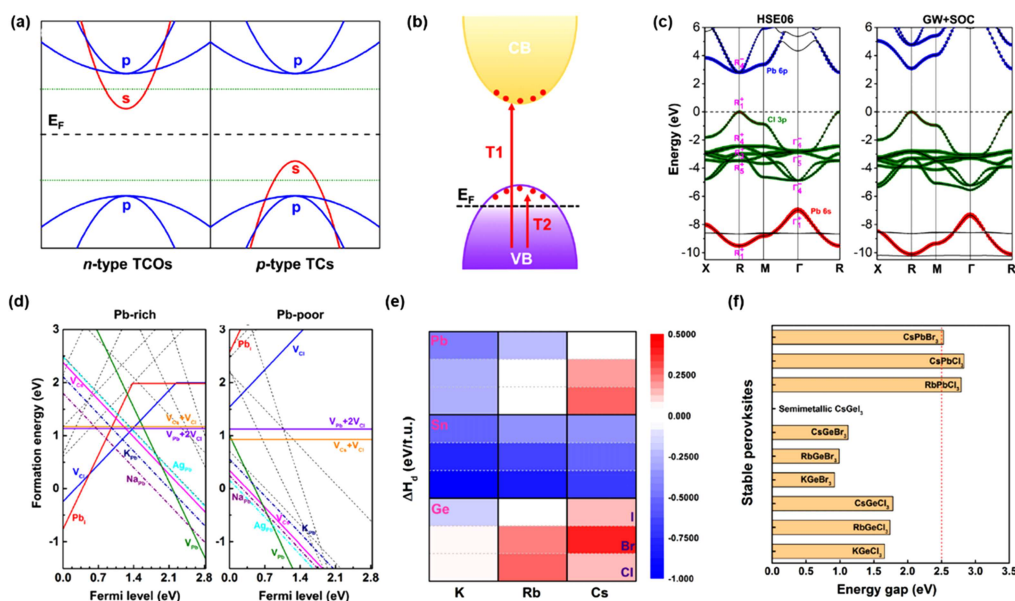


Fig. 14. (a) Schematic illustration of normal band structure for conventional n-type TCOs such as In₂O₃ and inverted band structure for p-type TCOs. The black dashed line indicates the position of Fermi level, while the green dotted lines present the doping-limit energy level. (b) Interband (T1) and intraband (T2) optical transitions in p-type TCOs. (c) Band structures of CsPbCl₃ calculated by HSE06 and GW+SOC methods. (d) Calculated formation energies for various intrinsic defects, two defect complexes, and three extrinsic defects (K_{Pb} , Na_{Pb} , and Ag_{Pb}) in CsPbCl₃, under both the Pb-rich and Pb-poor conditions. (e) Decomposition energies (ΔH_d) of 27 IMHPs. (f) Band gaps of 10 stable IMHPs, calculated with GW+SOC method. Modification with permission from Ref. [121].

4. Conclusion and perspectives

This review summarizes the theoretical works on the electronic structure, optical and defect properties of halide perovskites and the derived stable Pb-free optoelectronic materials. We show that by adopting compositional management and 3D to 2D structural conversion, the thermodynamic stability of Pb-based halide perovskites can be improved, which is beneficial to the application in the field of solar cell. Adopting cation transmutation with varied configuration and high-throughput screening of perovskite and spinel structure, series of stable and lead-free materials have been discovered and designed for solar cells and other optoelectronic applications such as electroluminescence, photodetector, x-ray imaging, laser, photocatalysis, and etc. However, in general, it is very difficult to simultaneously improve all the required material properties for specific applications, therefore, the greatest challenge in practical optoelectronic application using these materials would be the optimization of the material properties through band struc-

ture engineering and defect control. Our review shows that first-principles electronic structure calculations can provide us deep understanding on the material properties of perovskites. These understandings can help us design and study new stable nontoxic perovskite-derived materials.

Acknowledgment

We acknowledge the computational support from the Beijing Computational Science Research Center.

References

- [1] Hao J, Li W, Zhai J and Chen H 2019 *Mat. Sci. Eng. R* **135** 1
- [2] Cohen R E 1992 *Nature* **358** 136
- [3] Pena M and Fierro J 2001 *Chem. Rev.* **101** 1981
- [4] Kanhere P and Chen Z 2014 *Molecules* **19** 19995
- [5] Kojima A, Teshima K, Shirai Y and Miyasaka T 2009 *J. Am. Chem. Soc.* **131** 6050
- [6] Lee M M, Teuscher J, Miyasaka T, Murakami T N and Snaith H J 2012 *Science* **338** 643

- [7] Burschka J, Pellet N, Moon S J, Humphry-Baker R, Gao P, Nazeeruddin M K and Grätzel M 2013 *Nature* **499** 316
- [8] Liu M, Johnston M B and Snaith H J 2013 *Nature* **501** 395
- [9] Green M A, Ho-Baillie A and Snaith H J 2014 *Nat. Photonics* **8** 506
- [10] Zhou H, Chen Q, Li G, Luo S, Song T B, Duan H S, Hong Z, You J, Liu Y and Yang Y 2014 *Science* **345** 542
- [11] Saliba M, Matsui T, Domanski K, Seo J Y, Ummadisingu A, Zakeeruddin S M, Correa-Baena J-P, Tress W R, Abate A and Hagfeldt A 2016 *Science* **354** 206
- [12] Yang W S, Park B W, Jung E H, Jeon N J, Kim Y C, Lee D U, Shin S S, Seo J, Kim E K and Noh J H 2017 *Science* **356** 1376
- [13] Jeon N J, Na H, Jung E H, Yang T Y, Lee Y G, Kim G, Shin H W, Seok S I, Lee J and Seo J 2018 *Nat. Energy* **3** 682
- [14] Jiang Q, Zhao Y, Zhang X, Yang X, Chen Y, Chu Z, Ye Q, Li X, Yin Z and You J 2019 *Nat. Photonics* **13** 460
- [15] Jung E H, Jeon N J, Park E Y, Moon C S, Shin T J, Yang T-Y, Noh J H and Seo J 2019 *Nature* **567** 511
- [16] <https://www.nrel.gov/pv/assets/pdfs/best-research-cell-efficiencies.20200406.pdf>
- [17] Yin W J, Yang J H, Kang J, Yan Y and Wei S H 2015 *J. Mater. Chem. A* **3** 8926
- [18] De Wolf S, Holovsky J, Moon S J, Löper P, Niesen B, Ledinsky M, Haug F J, Yum J H and Ballif C 2014 *J. Phys. Chem. Lett.* **5** 1035
- [19] D'innocenzo V, Grancini G, Alcocer M J, Kandada A R S, Stranks S D, Lee M M, Lanzani G, Snaith H J and Petrozza A 2014 *Nat. Commun.* **5** 1
- [20] Wehrenfennig C, Eperon G E, Johnston M B, Snaith H J and Herz L M 2014 *Adv. Mater.* **26** 1584
- [21] Zhang X, Shen J X, Wang W and Van de Walle C G 2018 *ACS Energy Lett.* **3** 2329
- [22] Zhang X, Shen J X and Van de Walle C G 2019 *Adv. Energy Mater.*
- [23] Yin W J, Shi T and Yan Y 2014 *Appl. Phys. Lett.* **104** 063903
- [24] Walsh A, Scanlon D O, Chen S, Gong X and Wei S H 2015 *Angew. Chem., Int. Ed.* **54** 1791
- [25] Yin W J, Shi T and Yan Y 2014 *Advanced Materials* **26** 4653
- [26] Wang Q, Shao Y, Xie H, Lyu L, Liu X, Gao Y and Huang J 2014 *Appl. Phys. Lett.* **105** 163508
- [27] Agiorgousis M L, Sun Y Y, Zeng H and Zhang S 2014 *J Am Chem Soc* **136** 14570
- [28] Meggiolaro D, Motti S G, Mosconi E, Barker A J, Ball J, Perini C A R, Deschler F, Petrozza A and De Angelis F 2018 *Energy Environ. Sci.* **11** 702
- [29] Li J L, Yang J, Wu T and Wei S H 2019 *J. Mater. Chem. C* **7** 4230
- [30] Shi Z, Guo J, Chen Y, Li Q, Pan Y, Zhang H, Xia Y and Huang W 2017 *Adv. Mater.* **29** 1605005
- [31] Ono L K, Park N G, Zhu K, Huang W and Qi Y 2017 *ACS Energy Letters* **2** 1749
- [32] Niu G, Li W, Meng F, Wang L, Dong H and Qiu Y 2014 *J. Mater. Chem. A* **2** 705
- [33] Conings B, Drijkoningen J, Gauquelin N, Babayigit A, D'Haen J, D'Olieslaeger L, Ethirajan A, Verbeeck J, Manca J, Mosconi E, Angelis F D and Boyen H G 2015 *Adv. Energy Mater.* **5** 1500477
- [34] Zhang Y Y, Chen S, Xu P, Xiang H, Gong X G, Walsh A and Wei S-H 2018 *Chin. Phys. Lett.* **35** 036104
- [35] Li C, Lu X, Ding W, Feng L, Gao Y and Guo Z 2008 *Acta Crystallogr., Sect. B: Struct. Sci.* **64** 702
- [36] Marshall K, Walker M, Walton R and Hatton R 2016 *Nat. Energy* **1** 1
- [37] Hao F, Stoumpos C C, Cao D H, Chang R P and Kanatzidis M G 2014 *Nat. Photonics* **8** 489
- [38] Gu S, Lin R, Han Q, Gao Y, Tan H and Zhu J 2020 *Adv. Mater.* **32** 1907392
- [39] Kamarudin M A, Hirotani D, Wang Z, Hamada K, Nishimura K, Shen Q, Toyoda T, Iikubo S, Minemoto T and Yoshino K 2019 *J. Phys. Chem. Lett.* **10** 5277
- [40] Tavakoli M M, Zakeeruddin S M, Grätzel M and Fan Z 2018 *Adv. Mater.* **30** 1705998
- [41] Lin R, Xiao K, Qin Z, Han Q, Zhang C, Wei M, Saidaminov M I, Gao Y, Xu J and Xiao M 2019 *Nat. Energy* **4** 864
- [42] Zhao X G, Yang J H, Fu Y, Yang D, Xu Q, Yu L, Wei S H and Zhang L 2017 *J Am Chem Soc* **139** 2630
- [43] Sun Q, Wang J, Yin W J and Yan Y 2018 *Adv. Mater.* **30** 1705901
- [44] Li Z, Yang M, Park J S, Wei S H, Berry J J and Zhu K 2015 *Chem. Mater.* **28** 284
- [45] Yin W J, Yan Y and Wei S H 2014 *J. Phys. Chem. Lett.* **5** 3625
- [46] Huo Z, Wei S H and Yin W J 2018 *J. Phys. D: Appl. Phys.* **51** 474003
- [47] Lee J W, Seol D J, Cho A N and Park N G 2014 *Adv. Mater.* **26** 4991
- [48] Filip M R, Eperon G E, Snaith H J and Giustino F 2014 *Nat. Commun.* **5** 1
- [49] Bartel C J, Sutton C, Goldsmith B R, Ouyang R, Musgrave C B, Ghiringhelli L M and Scheffler M 2019 *Science Adv.* **5** eaav0693
- [50] Sun Q and Yin W J 2017 *J. Am. Chem. Soc.* **139** 14905
- [51] Saliba M, Matsui T, Seo J Y, Domanski K, Correa-Baena J P, Nazeeruddin M K, Zakeeruddin S M, Tress W, Abate A and Hagfeldt A 2016 *Energy Environ. Sci.* **9** 1989
- [52] Manser J S, Christians J A and Kamat P V 2016 *Chem. Rev.* **116** 12956
- [53] Tan H, Jain A, Voznyy O, Lan X, De Arquer F P G, Fan J Z, Quintero-Bermudez R, Yuan M, Zhang B and Zhao Y 2017 *Science* **355** 722
- [54] Saidaminov M I, Williams K, Wei M, Johnston A, Quintero-Bermudez R, Vafaie M, Pina J M, Proppe A H, Hou Y and Walters G 2020 *Nat. Mater.* **19** 412
- [55] Li Y, Zhang X, Huang H, Kershaw S V and Rogach A L 2020 *Mater. Today* **32** 204
- [56] Abdollahi Nejad B, Hossain I M, Jakoby M, Moghadamzadeh S, Abzieher T, Gharibzadeh S, Schwenzer J A, Nazari P, Schackmar F and Hauschild D 2020 *Adv. Energy Mater.* **10** 1902583
- [57] Colella S, Mosconi E, Fedeli P, Listorti A, Gazza F, Orlandi F, Ferro P, Besagni T, Rizzo A and Calestani G 2013 *Chem. Mater.* **25** 4613
- [58] Noh J H, Im S H, Heo J H, Mandal T N and Seok S I 2013 *Nano Lett.* **13** 1764
- [59] Edri E, Kirmayer S, Henning A, Mukhopadhyay S, Gartsman K, Rosenwaks Y, Hodes G and Cahen D 2014 *Nano Lett.* **14** 1000
- [60] Stranks S D, Eperon G E, Grancini G, Menelaou C, Alcocer M J, Leijtens T, Herz L M, Petrozza A and Snaith H J 2013 *Science* **342** 341
- [61] Edri E, Kirmayer S, Cahen D and Hodes G 2013 *J. Phys. Chem. Lett.* **4** 897
- [62] Edri E, Kirmayer S, Kulbak M, Hodes G and Cahen D 2014 *J. Phys. Chem. Lett.* **5** 429
- [63] Suarez B, Gonzalez-Pedro V, Ripolles T S, Sanchez R S, Otero L and Mora-Sero I 2014 *J. Phys. Chem. Lett.* **5** 1628
- [64] Zhao Y and Zhu K 2016 *Chem. Soc. Rev.* **45** 655
- [65] Beal R E, Slotcavage D J, Leijtens T, Bowring A R, Belisle R A, Nguyen W H, Burkhard G F, Hoke E T and McGehee M D 2016 *J. Phys. Chem. Lett.* **7** 746
- [66] Ono L K, Juarez-Perez E J and Qi Y 2017 *ACS Appl. Mater. Interfaces* **9** 30197
- [67] Jena A K, Kulkarni A and Miyasaka T 2019 *Chem. Rev.* **119** 3036
- [68] Righetto M, Meggiolaro D, Rizzo A, Sorrentino R, He Z, Meneghesso G, Sum T C, Gatti T and Lamberti F 2020 *Prog. Mater. Sci.* **110** 100639
- [69] McMeekin D P, Sadoughi G, Rehman W, Eperon G E, Saliba M, Hörantner M T, Haghighirad A, Sakai N, Korte L and Rech B 2016 *Science* **351** 151
- [70] Han Y, Zhao H, Duan C, Yang S, Yang Z, Liu Z and Liu S 2020 *Adv. Funct. Mater.* **30** 1909972
- [71] Kitazawa N, Watanabe Y and Nakamura Y 2002 *J. Mater. Sci.* **37** 3585
- [72] Perera S, Hui H, Zhao C, Xue H, Sun F, Deng C, Gross N, Milleville C, Xu X, Watson D F, Weinstein B, Sun Y-Y, Zhang S and Zeng H 2016 *Nano Energy* **22** 129
- [73] Sun Y Y, Agiorgousis M L, Zhang P and Zhang S 2015 *Nano Lett.* **15** 581
- [74] Nie R, Mehta A, Park B W, Kwon H W, Im J and Seok S I 2018 *J. Am. Chem. Soc.* **140** 872
- [75] Meng W, Saparov B, Hong F, Wang J, Mitzi D B and Yan Y 2016 *Chemistry of Materials* **28** 821
- [76] Perera S, Hui H, Zhao C, Xue H, Sun F, Deng C, Gross N, Milleville C, Xu X and Watson D F 2016 *Nano Energy* **22** 129
- [77] Niu S, Huyan H, Liu Y, Yeung M, Ye K, Blankemeier L, Orvis T, Sarkar D, Singh D J and Kapadia R 2017 *Advanced Materials* **29** 1604733
- [78] Wei X, Hui H, Perera S, Sheng A, Watson D F, Sun Y Y, Jia Q, Zhang S and Zeng H 2020 *ACS Omega* **5** 18579
- [79] Park J S, Yang J H, Kanevce A, Choi S, Repins I L and Wei S H 2015 *Physical Review B* **91** 075204
- [80] Walsh A, Chen S, Wei S H and Gong X G 2012 *Advanced Energy Materials* **2** 400
- [81] Chen S, Gong X, Walsh A and Wei S H 2009 *Phys. Rev. B* **79** 165211
- [82] Zhang P, Yang J and Wei S H 2018 *J. Mater. Chem. A* **6** 1809

- [83] Yang J, Zhang P and Wei S H 2018 *J. Phys. Chem. Lett.* **9** 31
- [84] Xiao Z, Du K-Z, Meng W, Wang J, Mitzi D B and Yan Y 2017 *J. Am. Chem. Soc.* **139** 6054
- [85] Lee B, Stoumpos C C, Zhou N, Hao F, Malliakas C, Yeh C Y, Marks T J, Kanatzidis M G and Chang R P 2014 *J. Am. Chem. Soc.* **136** 15379
- [86] Xiao Z, Zhou Y, Hosono H and Kamiya T 2015 *Phys. Chem. Chem. Phys.* **17** 18900
- [87] Maughan A E, Ganose A M, Bordelon M M, Miller E M, Scanlon D O and Neilson J R 2016 *J. Am. Chem. Soc.* **138** 8453
- [88] Saparov B, Sun J P, Meng W, Xiao Z, Duan H S, Gunawan O, Shin D, Hill I G, Yan Y and Mitzi D B 2016 *Chem. Mater.* **28** 2315
- [89] Filip M R, Hillman S, Haghighirad A A, Snaith H J and Giustino F 2016 *J. Phys. Chem. Lett.* **7** 2579
- [90] McClure E T, Ball M R, Windl W and Woodward P M 2016 *Chem. Mater.* **28** 1348
- [91] Slavney A H, Hu T, Lindenberg A M and Karunadasa H I 2016 *J. Am. Chem. Soc.* **138** 2138
- [92] Volonakis G, Filip M R, Haghighirad A A, Sakai N, Wenger B, Snaith H J and Giustino F 2016 *J. Phys. Chem. Lett.* **7** 1254
- [93] Volonakis G, Haghighirad A A, Milot R L, Sio W H, Filip M R, Wenger B, Johnston M B, Herz L M, Snaith H J and Giustino F 2017 *J. Phys. Chem. Lett.* **8** 772
- [94] Zhao X G, Yang D, Sun Y, Li T, Zhang L, Yu L and Zunger A 2017 *J. Am. Chem. Soc.* **139** 6718
- [95] Pan W, Wu H, Luo J, Deng Z, Ge C, Chen C, Jiang X, Yin W J, Niu G and Zhu L 2017 *Nat. Photonics* **11** 726
- [96] Luo J, Li S, Wu H, Zhou Y, Li Y, Liu J, Li J, Li K, Yi F, Niu G and Tang J 2018 *ACS Photonics* **5** 398
- [97] da Fonseca R, Sosman L, Tavares A D and Bordallo H 2000 *J. Fluoresc.* **10** 375
- [98] Aull B F and Jenssen H P 1986 *Phys. Rev. B* **34** 6647
- [99] Zhou L, Xu Y F, Chen B X, Kuang D B and Su C Y 2018 *Small* **14** 1703762
- [100] Nag A 2018 *Chem. Commun.* **54** 5205
- [101] Deng T, Song E, Zhou Y, Wang L and Zhang Q 2017 *J. Mater. Chem. C* **5** 12422
- [102] Tan Z, Li J, Zhang C, Li Z, Hu Q, Xiao Z, Kamiya T, Hosono H, Niu G and Lifshitz E 2018 *Adv. Funct. Mater.* **28** 1801131
- [103] Luo J, Wang X, Li S, Liu J, Guo Y, Niu G, Yao L, Fu Y, Gao L, Dong Q, Zhao C, Leng M, Ma F, Liang W, Wang L, Jin S, Han J, Zhang L, Etheridge J, Wang J, Yan Y, Sargent E H and Tang J 2018 *Nature* **563** 541
- [104] Slavney A H, Hu T, Lindenberg A M and Karunadasa H I 2016 *J. Am. Chem. Soc.* **138** 2138
- [105] McClure E T, Ball M R, Windl W and Woodward P M 2016 *Chemistry of Materials* **28** 1348
- [106] Ji F, Klarbring J, Wang F, Ning W, Wang L, Yin C, Figueroa J S M, Christensen C K, Etter M, Ederth T, Sun L, Simak S I, Abrikosov I A and Gao F 2020 *Angew. Chem., Int. Ed.* **59** 15191
- [107] Yang Y, Gao F, Gao S and Wei S-H 2018 *J. Mater. Chem. A* **6** 14949
- [108] Wang J, Chen H, Wei S H and Yin W J 2019 *Adv. Mater.* **31** e1806593
- [109] Smith I C, Hoke E T, Solis-Ibarra D, McGehee M D and Karunadasa H I 2014 *Angew. Chem., Int. Ed.* **53** 11232
- [110] Quan L N, Yuan M, Comin R, Voznyy O, Beauregard E M, Hoogland S, Buin A, Kirmani A R, Zhao K and Amassian A 2016 *J. Am. Chem. Soc.* **138** 2649
- [111] Tsai H, Nie W, Blancon J C, Stoumpos C C, Asadpour R, Harutyunyan B, Neukirch A J, Verduzco R, Crochet J J and Tretiak S 2016 *Nature* **536** 312
- [112] Liu J, Xue Y, Wang Z, Xu Z Q, Zheng C, Weber B, Song J, Wang Y, Lu Y and Zhang Y 2016 *ACS Nano* **10** 3536
- [113] Yang J H, Yuan Q and Yakobson B I 2016 *J. Phys. Chem. C* **120** 24682
- [114] Huang K, Lai K, Yan C-L and Zhang W-B 2017 *J. Chem. Phys.* **147** 164703
- [115] Green M A, Dunlop E D, Levi D H, Hohl-Ebinger J, Yoshita M and Ho-Baillie A W Y 2019 *Prog. Photovolt. Res. Appl.* **27** 565
- [116] Deng H X, Wei S H, Li S S, Li J and Walsh A 2013 *Phys. Rev. B* **87** 125203
- [117] Deng H X, Luo J W and Wei S H 2018 *Chin. Phys. B* **27** 117104
- [118] Kim J, Lee S H, Lee J H and Hong K H 2014 *J. Phys. Chem. Lett.* **5** 1312
- [119] Du M H 2015 *J. Phys. Chem. Lett.* **6** 1461
- [120] Haque M A, Li J L, Abdelhady A L, Saidaminov M I, Baran D, Bakr O M, Wei S H and Wu T 2019 *Adv. Opt. Mater.* **7** 1900865
- [121] Zhang P, Yu S, Zhang X and Wei S H 2019 *Phys. Rev. Mater.* **3** 055201
- [122] Wang R, Zhang X, He J, Ma C, Xu L, Sheng P and Huang F 2017 *J. Alloys Compd.* **695** 555
- [123] Abdelhady A L, Saidaminov M I, Murali B, Adinolfi V, Voznyy O, Katsiev K, Alarousu E, Comin R, Dursun I and Sinatra L 2016 *J. Phys. Chem. Lett.* **7** 295
- [124] Yamada Y, Hoyano M, Akashi R, Oto K and Kanemitsu Y 2017 *J. Phys. Chem. Lett.* **8** 5798
- [125] Nayak P K, Sendner M, Wenger B, Wang Z, Sharma K, Ramadan A J, Lovrinčić R, Pucci A, Madhu P and Snaith H J 2018 *J. Am. Chem. Soc.* **140** 574
- [126] Zhang S and Chadi D 1990 *Phys. Rev. B* **42** 7174
- [127] Chadi D and Chang K J 1988 *Phys. Rev. Lett.* **61** 873
- [128] Thio T, Bennett J and Becla P 1996 *Phys. Rev. B* **54** 1754
- [129] Espinosa F, de Leon J M, Conradson S, Pena J and Zapata-Torres M 1999 *Phys. Rev. Lett.* **83** 3446
- [130] Wei S-H and Zhang S 2002 *Phys. Rev. B* **66** 155211
- [131] Wang J, Li W and Yin W J 2020 *Adv. Mater.* **32** 1906115
- [132] Ulatowski A M, Wright A D, Wenger B, Buizza L R, Motti S G, Eggimann H J, Savill K J, Borchert J, Snaith H J and Johnston M B 2020 *J. Phys. Chem. Lett.* **11** 3681
- [133] Chopra K, Major S and Pandya D 1983 *Thin Solid Films* **102** 1
- [134] Nomura K, Ohta H, Ueda K, Kamiya T, Hirano M and Hosono H 2003 *Science* **300** 1269
- [135] Wager J F 2003 *Science* **300** 1245
- [136] Nomura K, Ohta H, Takagi A, Kamiya T, Hirano M and Hosono H 2004 *Nature* **432** 488
- [137] Minami T 2005 *Semicond. Sci. Technol.* **20** S35
- [138] Granqvist C G 2007 *Sol. Energy Mater. Sol. Cells* **91** 1529
- [139] Zhang K H, Xi K, Blamire M G and Egdell R G 2016 *J. Phys.: Condens. Matter* **28** 383002